Supporting Material for: Determining the Gaussian curvature modulus of lipid membranes in simulations

Mingyang Hu, John Briguglio, and Markus Deserno*
Department of Physics, Carnegie Mellon University, Pittsburgh, Pennsylvania

February 28, 2012

1 Simulation setup

1.1 Lipid Model

We use the solvent-free coarse-grained lipid model due to Cooke *et al.* (1, 2). A lipid is represented by three linearly connected beads, one for the head and two for the tails. Bead sizes are fixed by a Weeks-Chandler-Andersen potential

$$V_{\rm rep}(r;b) = \begin{cases} 4\epsilon\left[(\frac{b}{r})^{12} - (\frac{b}{r})^{6} + \frac{1}{4}\right] & , \ r \le r_{\rm c} \\ 0 & , \ r > r_{\rm c} \end{cases} , \tag{S1}$$

with $r_{\rm c} = 2^{1/6} b$ and ϵ the unit of energy. To ensure a cylindrical lipid shape, $b_{\rm head,head} = b_{\rm head,tail} = 0.95\,\sigma$ and $b_{\rm tail,tail} = \sigma$, where σ is the unit of length. The three beads are linked by two FENE bonds

$$V_{\rm bond}(r) = -\tfrac{1}{2} k_{\rm bond}\, r_\infty^2 \log\left[1 - (r/r_\infty)^2\right] , \tag{S2}$$

with $k_{\rm bond} = 30\,\epsilon/\sigma^2$ and $r_\infty = 1.5\,\sigma$. To keep lipids essentially straight, the two end beads are pushed apart with a harmonic bond of rest length 4σ:

$$V_{\rm bend}(r) = \tfrac{1}{2} k_{\rm bend}(r - 4\sigma)^2 . \tag{S3}$$

To lowest order this is equivalent to a harmonic bending potential $\frac{1}{2} k_{\rm bend}\sigma^2\,\vartheta^2$ for the angle $\pi - \vartheta$ between the three beads. The value of the bending stiffness is $k_{\rm bend}\sigma^2 = 10\,\epsilon$. To achieve aggregation in the absence of any solvent, all *tail* beads attract according to

$$V_{\rm attr}(r) = \begin{cases} -\epsilon & , \quad r < r_{\rm c} \\ -\epsilon\,\cos^2\frac{\pi(r-r_{\rm c})}{2w_{\rm c}} & , \ r_{\rm c} \le r \le r_{\rm c} + w_{\rm c} \\ 0 & , \quad r > r_{\rm c} + w_{\rm c} \end{cases} , \tag{S4}$$

This attractive potential has a well of depth ϵ and for $r > r_{\rm c}$ smoothly tapers to zero. The range parameter $w_{\rm c}$ is crucial in obtaining fluid phases: If it is too short, the condensed phase is invariable a gel or a crystal, but not a fluid bilayer. In fact, for $w_{\rm c} \simeq 0.7$ the range of attraction is similar to the ubiquitous Lennard-Jones potential and in this case no fluid phase region exists.

Notice that this attraction pulls the tail beads closer together, but not the head beads. In order to still have a roughly cylindrical lipid shape, the head bead is 5% smaller than the two tail beads. Changing the head bead size can indeed be used to affect the lipid curvature, as previously shown (3).

*Corresponding author. Address: Department of Physics, Carnegie Mellon University, 5000 Forbes Avenue, Pittsburgh, PA 15213, U.S.A., Tel.: (412)268-4401, Fax: (412)681-0648

1.2 Simulation engine

We performed Molecular Dynamics (MD) simulations using the ESPResSo package (4). The temperature was set by a Langevin thermostat (5) (with a time step $\delta t = 0.01\,\tau$ and a friction constant $\Gamma = 1.0\,\tau^{-1}$ in Lennard-Jones units).

2 Determining the other membrane properties

2.1 Bending modulus

The bending modulus κ was determined by the method of Harmandaris and Deserno (6). Briefly, a cylindrical bilayer tube is created which spans across the periodic boundary conditions of the simulation box, say along the z-axis. If this tube has length L_z and (midplane) radius R, and thus area $A = 2\pi R L_z$, the curvature energy is given by

$$E_{\mathrm{bend}} = A \times \frac{1}{2}\kappa\frac{1}{R^2} = \frac{1}{2}\kappa\frac{(2\pi L_z)^2}{A} \ . \tag{S5}$$

This tube exerts a tensile force f along its axis, given by the derivative of the energy with respect to length at constant area:

$$f = \left(\frac{\partial R_{\mathrm{bend}}}{\partial L_z}\right)_A = \frac{2\pi\kappa}{R} \ , \tag{S6}$$

From which κ can be determined. This procedure works even if the radius of curvature is not much bigger than the bilayer thickness (6). We always determined κ by using curvature radii that matched the radii relevant in the crossover region of the folding-up simulations.

2.2 Edge tension

The edge tension γ was determined by simulating a flat bilayer which spans only in one direction across the periodic boundary condition of the simulation box (say, the x direction) but not in the other two directions. It therefore will have two open edges along which a tension pulls. Measuring the stress along the x direction and multiplying by the perpendicular box area $L_y L_z$ gives the force f, and dividing this by 2 then gives the edge tension γ.

2.3 Area

The area was inferred from the number of lipids and the equilibrium area per lipid at zero tension. In contrast to the determination of the bending modulus κ and the edge tension γ this procedure is very accurate, so we dispensed with an accurate error determination (it in any case appears to be much smaller than 1%).

3 Implementation of folding simulations

3.1 Creating the initial configuration

To create the pre-curved initial configuration, we turn on an artificial spherically symmetric external potential that creates a "groove" of curvature radius c^{-1} for the outer tail-beads of all lipids. Its functional form is

$$V_{\mathrm{groove}}(r) = \begin{cases} V_0\left[\left(\dfrac{r-c^{-1}}{d}\right)^2 - 1\right] & , \quad |r-c^{-1}| < d \\ 0 & , \quad \text{otherwise} \end{cases} \tag{S7}$$

The depth of this potential is $V_0 = 0.5\,\epsilon$, and the maximum elongation is $d = 1.5\,\sigma$.

The strength of this perturbation suffices to force an initially flat membrane patch into a spherically curved one with curvature c, but it remains weak enough not to disturb the overall membrane structure. We then let this bilayer relax for about $100\,\tau$, permitting the area per lipid on both leaflets to equilibrate

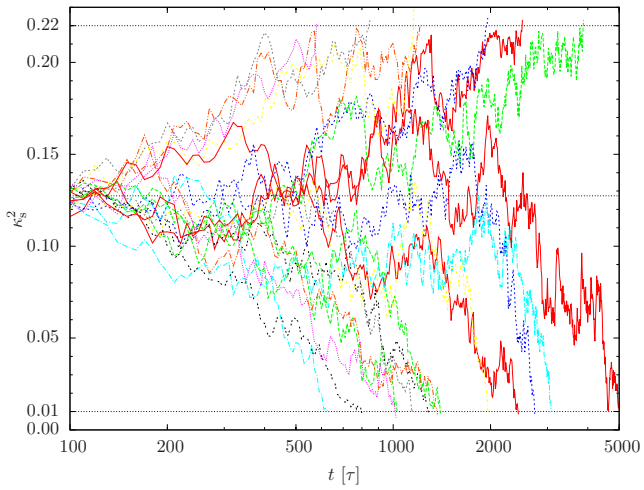

Figure S1: Time-traces of the shape anisotropy κ_s^2 for 20 randomly chosen individual simulations of system 1, initially constrained to lie on a spherical shell with radius $9.72\,\sigma$ (corresponding to $x = 0.456$) via the groove-potential from Eq. S7, which is then turned off at $t = 100\,\tau$. As Fig. 1 in the main paper shows, the closing-up probability in this case is about 60%; here we see that 13 out of 20 simulations close up, which is already quite close to this probability. Notice also that even when only looking at 20 trajectories, the closing-up times already vary over at least one order of magnitude, which is why it is advantageous to terminate a simulation once the fate of the disc is clear, and not after a predetermined (possibly large) time has passed.

over the open rim. After this, the external field V_{groove} is removed and we then follow the evolution of the pre-curved patch.

3.2 Identifying the final state

By eye, it is trivial to see whether a pre-curved bilayer patch (ultimately) opens up or folds into a vesicle. However, since we do these simulations hundreds of times, we need an automated criterion for determining the fate of the patch. We decided to monitor a shape parameter constructed from the gyration tensor of the patch.

Briefly, we calculate the gyration tensor

$$\mathbf{Q} = \frac{1}{N}\sum_{i=1}^{N}(\boldsymbol{r}_i - \boldsymbol{r}_{\text{cm}}) \otimes (\boldsymbol{r}_i - \boldsymbol{r}_{\text{cm}}) \ , \tag{S8}$$

where $\boldsymbol{r}_{\text{cm}} = \frac{1}{N}\sum_{i=1}^{N}\boldsymbol{r}_i$ is the center of mass and where the sums run over all N beads in our system. Let us call the three eigenvalues of this tensor $\lambda_1^2 \le \lambda_2^2 \le \lambda_3^2$. Following Theodorou and Suter (7), we define a number of invariants that help to characterize the shape, namely: the *radius of gyration* R_{g}^2, the *asphericity* b, the *acylindricity* c, and the *relative shape anisotropy* κ_{s}^2:

$$R_{\text{g}}^2 = \lambda_1^2 + \lambda_2^2 + \lambda_3^2 \ , \tag{S9a}$$

$$b = \lambda_3^2 - \frac{1}{2}(\lambda_1^2 + \lambda_2^2) \ , \tag{S9b}$$

$$c = \lambda_2^2 - \lambda_1^2 \ , \tag{S9c}$$

$$\kappa_{\text{s}}^2 = \frac{b^2 + \frac{3}{4}c^2}{R_{\text{g}}^4} \ . \tag{S9d}$$

For a spherical distribution $\kappa_{\text{s}}^2 = 0$, while for an infinitely thin circular disc $\kappa_{\text{s}}^2 = \frac{1}{4}$. These "ideal" values are never truly reached, because a closed-up vesicle is neither perfectly spherically symmetric (for instance

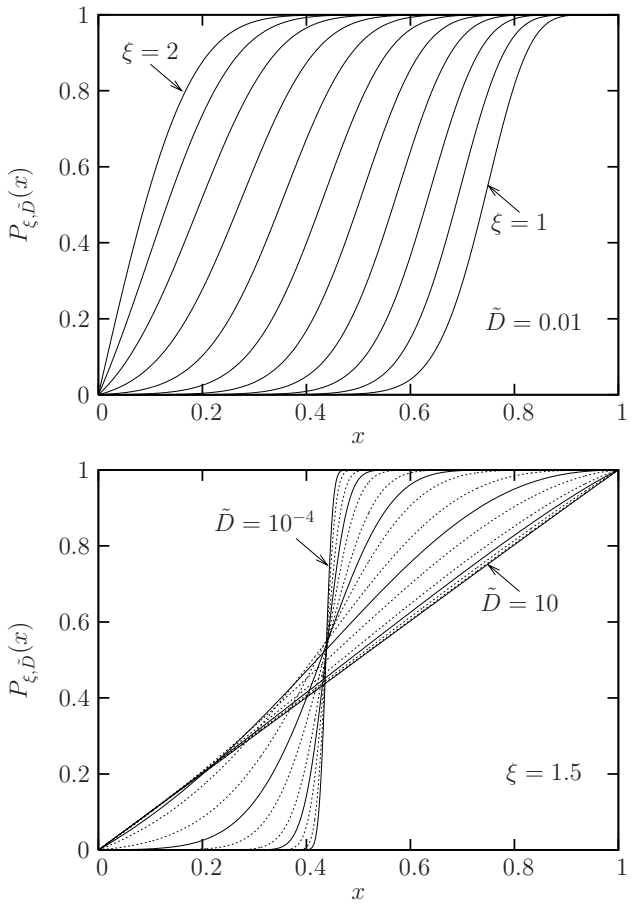

Figure S2: Illustration of the functional form of the splitting probability $P_{\xi,\tilde{D}}(x)$ as its two parameters ξ and $\tilde{D}$ are varied. The upper panel shows $P_{\xi,\tilde{D}}(x)$ for $\tilde{D} = 0.01$ and $\xi = 1 \ldots 2$ in steps of 0.1. The lower panel shows $P_{\xi,\tilde{D}}(x)$ for $\xi = 1.5$ and $\tilde{D} \in \{0.0001, 0.0002, 0.0005, 0.001, \ldots, 10\}$. To a large degree, ξ determines the location of the crossover, while $\tilde{D}$ determines its "sharpness". Notice, however, that $P_{\xi,\tilde{D}}(x)$ is *not* point-symmetric about the transition point and that *only* in the limit $\tilde{D} \to 0$ the transition coincides with the location where $P_{\xi,\tilde{D}} = \frac{1}{2}$.

because of thermal undulations), nor is a flat disc infinitely thin. However, we found that once $\kappa_s^2 < 0.01$, we can safely assume that the closed-up state has been (or will very soon be) reached, while for $\kappa_s^2 > 0.22$, the flat disc state has been reached. Once this has happened, we stop our simulation and remember the final outcome. Figure S1 shows 20 time-traces of κ_s^2 for system 1, constrained initially to a curvature radius of $9.72\,\sigma$ (corresponding to $x = 0.456$). This illustrate both the suitability of our automated decision criterion, as well as the fact that trajectories indeed can diffuse back and forth a while before settling on the final state.

3.3 Fitting to the splitting probability

As explained in the main article, the closing-up probability can be written analytically as (8)

$$P_{\xi,\tilde{D}}(x) = \frac{\int_0^x \mathrm{d}y \; \mathrm{e}^{\Delta\tilde{E}(y,\xi)/\tilde{D}}}{\int_0^1 \mathrm{d}y \; \mathrm{e}^{\Delta\tilde{E}(y,\xi)/\tilde{D}}} \;, \tag{S10}$$

where the scaled energy is given by

$$\Delta\tilde{E}(x,\xi) = x + \xi\left[\sqrt{1-x} - 1\right] \ , \tag{S11}$$

and the variables ξ and $\tilde{D}$ are the two fitting parameters. As it turns out, the integrals entering Eq. S10 can be solved analytically, and this leads to the following closed expression for the closing-up probability:

$$P_{\xi,\tilde{D}}(x) \ = \ \frac{2\sqrt{\tilde{D}}\,A(x) + \sqrt{\pi}\,\xi\,B\,[C + D(x)]}{2\sqrt{\tilde{D}}\,A(1) + \sqrt{\pi}\,\xi\,B\,[C + D(1)]} \ , \tag{S12}$$

where we defined the abbreviations

$$A(x) \ = \ \exp\left\{\frac{\xi}{\tilde{D}}\right\} - \exp\left\{\frac{x + \xi\sqrt{1-x}}{\tilde{D}}\right\} \ , \tag{S13a}$$

$$B \ = \ \exp\left\{\frac{4+\xi^2}{4\tilde{D}}\right\} \ , \tag{S13b}$$

$$C \ = \ \mathrm{erf}\left\{\frac{\xi - 2}{2\sqrt{\tilde{D}}}\right\} \ , \tag{S13c}$$

$$D(x) \ = \ \mathrm{erf}\left\{\frac{2\sqrt{1-x} - \xi}{2\sqrt{\tilde{D}}}\right\} \ . \tag{S13d}$$

Figure S2 illustrates the functional form of $P_{\xi,\tilde{D}}(x)$ as the two parameters ξ and $\tilde{D}$ are varied.

There is no principle difficulty to fit this function to the measured data for the closing-up probability, and thereby extract the value of ξ, from which in turn $\overline{\kappa}$ follows. To illustrate the quality of all our data, Fig. S3 illustrates the fits resulting for all the systems we have studied (see Table 2 in the main article for details about the systems' definition).

3.4 Error analysis

The folding simulations are effectively a sequence of Bernoulli trials, each of which succeeds (say, folds up) with a probability p. If N_{fold} of the N_{sim} simulations fold up, then $p^* = N_{\mathrm{fold}}/N_{\mathrm{sim}}$ is an unbiased and consistent estimator for p. And since we know that N_{fold} follows a Bernoulli distribution, the standard deviation of p^* is $\Delta p^* = \sqrt{p^*(1-p^*)/N_{\mathrm{sim}}}$.

After having values (and error bars) for the folding probability at varying values of x, we fit the splitting probability from Eq. S12 to these data to determine ξ. The error bar is determined by a Monte Carlo error analysis (9), in which a large number of artificial data sets are created in the following way: Each measured $p^*(x_i)$ is replaced by $p^*(x_i) + g_i\,\Delta p^*(x_i)$, where the g_i are Gaussian random numbers with zero mean and unit variance, and the $\Delta p^*(x_i)$ are the previously calculated (Bernoulli) errors in the measured values $p^*(x_i)$. This artificial data set was not derived from our simulations, but the error bars tell us that it *could have been*. We fit again and determine a new value of ξ. Repeating this process hundreds of times we get a distribution function for ξ, whose mean and standard deviation we subsequently quote as the measured value of ξ and its error, respectively.

3.5 Constraints on system parameters

The proposed method for determining $\overline{\kappa}$ only works if the material parameters satisfy certain constraints. First, for a barrier to exist, we must have $\xi < 2$ and thus

$$\frac{\gamma R}{2\kappa + \overline{\kappa}} \ = \ \frac{R}{\ell} < 2 \ , \tag{S14}$$

where we defined the characteristic length

$$\ell \ := \ \frac{2\kappa + \overline{\kappa}}{\gamma} \ . \tag{S15}$$

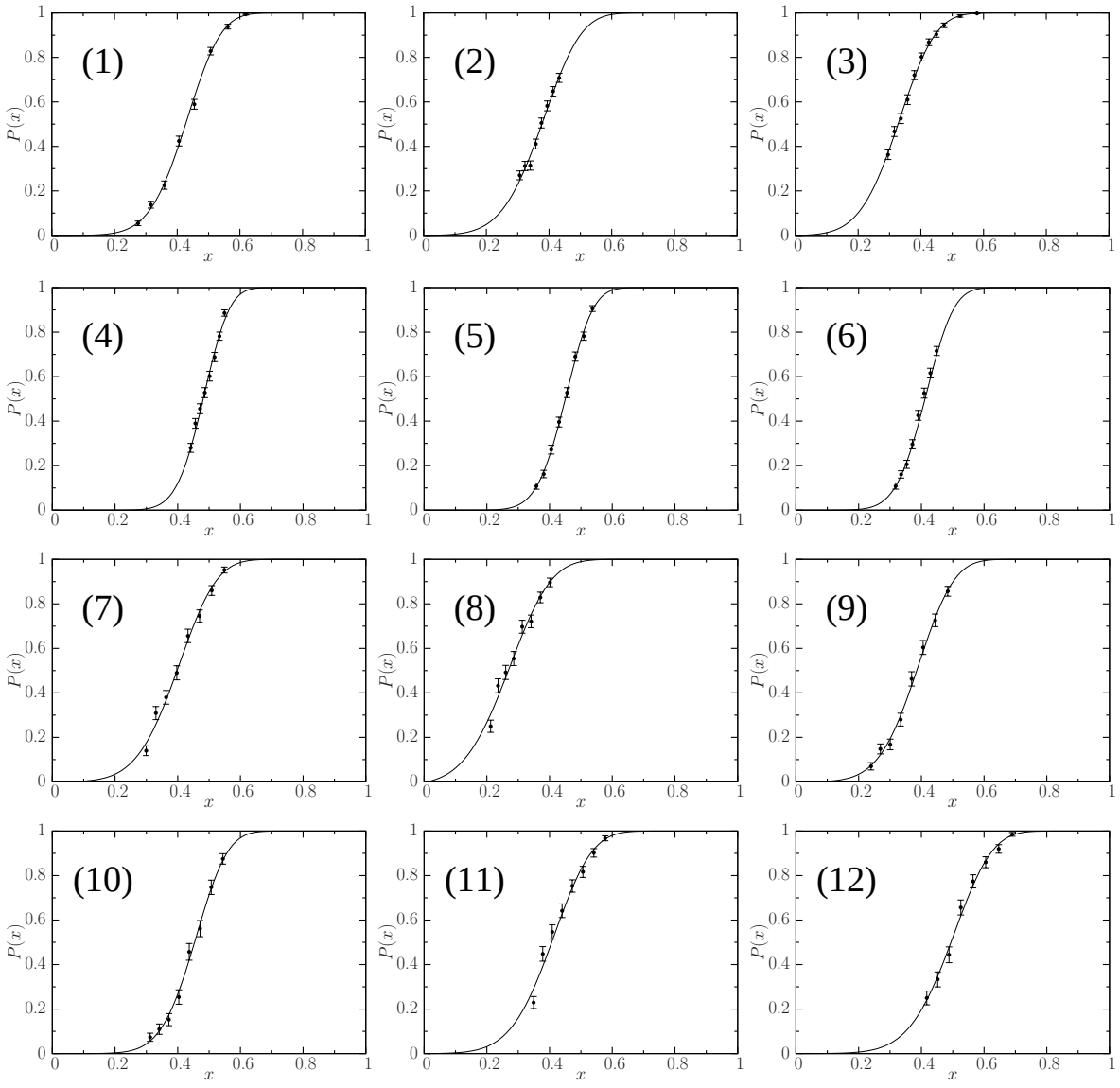

Figure S3: Figure 1 in the main paper illustrates the folding probability of the simulations done for system 1, as well as the fit to the splitting probability $P_{\xi,\tilde{D}}(x)$ from Eq. S12. This figure here shows the same plot for all 12 systems we studied. The number refers to the system number as indicated in Table 2 of the main paper.

Hence, ℓ must be sufficiently big, meaning that the "total" bending rigidity $2\kappa + \overline{\kappa}$ must be sufficiently big, or the edge tension γ sufficiently small.

What does it mean that ℓ must be bigger than $R/2$? Can we not always make R small enough by choosing a sufficiently small patch size $A = 4\pi R^2$? No, because there is a lower bound for that patch size: too highly curved membranes might no longer follow simple quadratic curvature elasticity. For instance, with $2\kappa + \overline{\kappa} \simeq 20\, k_\mathrm{B}T$ and a typical edge tension of 10 pN we get $\ell \simeq 8\,\mathrm{nm}$ Hence, R can be at most 16 nm. This is realistic, though, because curvature elasticity appears to work well down to curvature radii of a few times the membrane diameter ($\sim 4\,\mathrm{nm}$) (10). If, on the other hand, the lipids have a sufficiently negative spontaneous curvature, this makes edges very expensive and the edge tension might increase to, say, 40 pN. In this case R can be at most 4 nm, and this is problematic.

One might want the barrier $\Delta E^* = \pi(2\kappa+\overline{\kappa})(2-\xi)^2$ not only to exist but to be at least of some minimal height, say $\alpha\, k_\mathrm{B}T$ with α equal to "a few". As long as both $2\kappa+\overline{\kappa}$ and γR are large compared to $k_\mathrm{B}T$, which they almost certainly are, one finds a correction of

$$\ell \;\gtrsim\; \frac{R}{2}\left[1 + \frac{1}{2}\sqrt{\frac{\alpha\, k_\mathrm{B}T}{\pi(2\kappa+\overline{\kappa})}}\right] \;. \tag{S16}$$

With $2\kappa + \overline{\kappa} \simeq 20\, k_\mathrm{B}T$ and $\alpha = 4$ we get $\ell \geq 0.56\, R$, and for $2\kappa + \overline{\kappa} \simeq 10\, k_\mathrm{B}T$ and $\alpha = 5$ we get $\ell \geq 0.6\, R$. Neither are very big modifications to the simple estimate from Eq. S14. Notice finally that we do not actually rely on curving the disc up to the final vesical curvature radius R. The most important shapes in our simulations are those close to the barrier, and their curvature radius is given by $c_\mathrm{barrier}^{-1} = R[1-(\xi/2)^2]^{-1/2}$. Since ξ in our simulations tends to be around 1.5, this means that the most important curvature radius is actually about 50% bigger than R.

On the other hand, we also don't want the characteristic length ℓ to be too big, because this leads to fairly big membrane patches. These show substantial thermal fluctuations, and therefore the simple ground state theory underlying our analysis might become problematic. For instance, the folding-up pathway may not be axisymmetric, or not even follow a sequence of average shapes which are spherical caps. This situation might occur if the lipids have a sufficiently large positive spontaneous curvature so that they conform to bilayer edges very well and the edge tension drops a lot.

For the systems we have been simulating the value of ℓ tends to be around $4.4\,\sigma$ (which is approximately the membrane diameter). However, system 8 (with its more negative spontaneous lipid curvature) has a value of about $3.4\,\sigma$. While our previous measurements of the bending rigidity κ show that quadratic curvature elasticity is a good theory even at such high curvatures (6), at the very high accuracy at which we're aiming here a slight decrease of the apparent bending rigidity is noticeable. In other words, quartic corrections become visible. Unfortunately, there is not much we can do about this: While it is certainly possible to extend Helfrich theory to quartic terms, the problem is that there are four new terms to be considered (K^4, $K^2 K_\mathrm{G}$, K_G^2, and $(\nabla K)^2$), each with its own new modulus, and these moduli would then need to be determined *as well* before we can extract the modulus $\overline{\kappa}$ on the quadratic level. Since this pathway is not practicable at present, we must simply acknowledge that there are hard to quantify *systematic* deviations entering the determination of κ, and we must suspect that drifts of the same order of magnitude enter $\overline{\kappa}$ as well. One might hope that these drifts go into the same direction and would thus cancel in the elastic ratio $\overline{\kappa}/\kappa$, but it is not entirely obvious that this should be so.

4 Elastic parameters from the stress profile

4.1 A few theoretical preliminaries

The distribution of stress throughout a lipid bilayer contains information about some of its elastic parameters. If we assume that the bilayer lies in the xy-plane, at $z = 0$, then by symmetry the local pressure tensor $\Pi_{ij}(\boldsymbol{r})$ can only depend on z. Furthermore, since mechanical stability requires

$$\partial_i\, \Pi_{ij} = 0 \;, \tag{S17}$$

and since in the xyz-coordinate system, again by symmetry, the pressure tensor is diagonal, this reduces to

$$\partial_z \Pi_{zz}(z) \;=\; 0 \quad \text{or} \quad \Pi_{zz}(z) \;=\; \text{const.} \tag{S18}$$

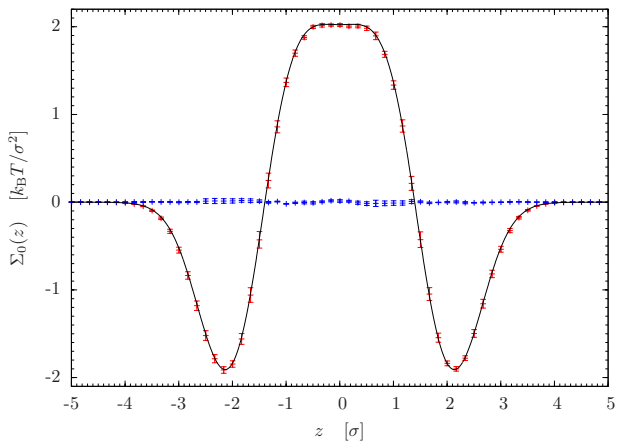

Figure S4: Lateral component $\Sigma_0(z)$ (red symbols) and normal component $\Sigma_\perp(z)$ (blue symbols) of the membrane stress. While the normal component is virtually constant (and zero, because for a solvent free model the pressure is zero away from the membrane), the lateral component has a nontrivial structure. The black solid line is a fit to the functional form from Eq. S24.

In contrast, the lateral component $\Pi_{xx}(z) = \Pi_{yy}(z)$ has a nontrivial functional form. In the membrane context one typically defines the stress as minus the pressure and introduces the two independent eigenvalues

$$\Sigma_{||}(z) = -\frac{1}{2}\Big(\Pi_{xx}(z) + \Pi_{yy}(z)\Big) , \tag{S19a}$$

$$\Sigma_\perp = -\Pi_{zz} . \tag{S19b}$$

If we further define

$$\Sigma_0(z) = \Sigma_{||}(z) - \Sigma_\perp , \tag{S20}$$

then this local lateral stress is only nonzero in the inhomogeneous region of the membrane, but vanishes in the bulk. The lateral membrane tension is then given by (11)

$$\Sigma = \int_{-\infty}^{\infty} \mathrm{d}z\, \Sigma_0(z) . \tag{S21}$$

Using mechanical arguments (12, 13) or an underlying microscopic membrane model (14), one can now relate higher moments of the stress profile $\Sigma_0(z)$ (of the *undeformed* bilayer!) to elastic parameters. In the tensionless state, $\Sigma = 0$, one finds for the entire bilayer bilayer

$$\overline{\kappa} = \int_{-\infty}^{\infty} \mathrm{d}z\, z^2\, \Sigma_0(z) , \tag{S22}$$

while on the monolayer level one gets

$$-\kappa_\mathrm{m} K_{0\mathrm{m}} = \int_{0}^{\infty} \mathrm{d}z\, (z - z_0)\, \Sigma_0(z) , \tag{S23a}$$

$$\overline{\kappa}_\mathrm{m} = \int_{0}^{\infty} \mathrm{d}z\, (z - z_0)^2\, \Sigma_0(z) , \tag{S23b}$$

where z_0 is the distance of the surface of inextenion of a monolayer from the bilayer midplane.

4.2 Stress profile from the simulation

Figure S4 shows the bilayer stress profile for system $1-3$ (from Table 2 in the main article). The convention followed to define the local stress is due to Irving and Kirkwood (15). It has been pointed out that defining

local stresses involves ambiguities, in the sense that if one only demands of the stress tensor that it satisfies the necessary conservation laws (and thus its divergence correctly links to the rate of change of the momentum density), it is not unique (11, 16). However Wajnryb *et al.* have argued that amending these by further plausible and physical conditions (*e. g.* pertaining to symmetry), the Irving-Kirkwood formula becomes unique (17), and so we follow this convention.

It can be seen in Fig. S4 that the normal component $\Sigma_\perp$ is indeed constant across the bilayer, as it should, and that the lateral component $\Sigma_0(z)$ shows nontrivial structure. It is positive in the center of the bilayer, because this is where in the Cook model (1, 2) the cohesion between the lipids happens, while it is negative at the head groups due to the purely repulsive interactions between them. We point out that this functional form is quite different from what one would expect for a real bilayer, where both in the tail and in the head region the repulsion dominates and $\Sigma_0(z)$ should be negative, while the cohesion should be localized to the interface region between head and tails.

Since we need to calculate moments of $\Sigma_0(z)$, we first fit the data to a suitable (but otherwise arbitrary) function. It turns out that a very good fit can be achieved with the functional form

$$f_N(x) \;=\; \frac{\sum_{i=0}^{N} a_{N,i} z^{2i}}{\exp\{c_{N,1}(z^2 - c_{N,2}^2)\} + 1 + \sum_{i=1}^{N} a_{N,i} z^{2i}} \tag{S24}$$

where $a_{N,0} \ldots c_{N,2}$ are fitting parameters. We tried $N \in \{2, 3, 4\}$ and found virtually identically good fits (in the sense that data minus fit is flat). By simulating two systems which very slightly differ in the area per lipid, we created two almost indistinguishable stress profiles, but one with a very slight positive tension, the other one with a slight negative tension. By a suitable convex combination of both profiles we can thus create a stress profile whose integral exactly vanishes, thus avoiding any potential artifacts due to a residual tension. The corresponding fit is shown as the black line in Fig. S4.

For the bilayer we then find the second moment through a straightforward numerical integration:

$$\int_{-\infty}^{\infty} \mathrm{d}z \; z^2 \, \Sigma_0(z) \;\simeq\; -21.7 \, k_\mathrm{B}T \;, \tag{S25}$$

and for the monolayer we can calculate the first moment without knowing z_0 (since the total $\Sigma = 0$):

$$\begin{aligned} &\int_{0}^{\infty} \mathrm{d}z \; (z - z_0) \, \Sigma_0(z) \\ =\;& \int_{0}^{\infty} \mathrm{d}z \; z \, \Sigma_0(z) \;\simeq\; -3.75 \, k_\mathrm{B}T/\sigma \;. \end{aligned} \tag{S26}$$

The second moment of the monolayer depends on the value of z_0, which we do not know a priori. It turns out that for $z_0 \simeq 1.445$ the second moment vanishes, and expanding about this point to linear order we find with very good accuracy

$$\int_{0}^{\infty} \mathrm{d}z \; (z - z_0)^2 \, \Sigma_0(z) \;\simeq\; 7.51 \, k_\mathrm{B}T \, (z_0/\sigma - 1.445) \;. \tag{S27}$$

This reproduces our estimated monolayer Gaussian curvature modulus $\overline{\kappa}_\mathrm{m} \approx -0.93 \times 12.44/2 = -5.78 \, k_\mathrm{B}T$ for $z_0 \simeq 0.68 \, \sigma$, which is implausibly small.

Supporting References

1. Cooke, I. R., K. Kremer, and M. Deserno, 2005. Tunable generic model for fluid bilayer membranes. *Phys. Rev. E* 72:011506.

2. Cooke, I. R., and M. Deserno, 2005. Solvent-free model for self-assembling fluid bilayer membranes: Stabilization of the fluid phase based on broad attractive tail potentials. *J. Chem. Phys.* 123:224710.

3. Cooke, I. R., and M. Deserno, 2006. Coupling between lipid shape and membrane curvature. *Biophys. J.* 91:487–495.

4. Limbach, H.-J., A. Arnold, B. A. Mann, and C. Holm, 2006. ESPResSo – An Extensible Simulation Package for Research on Soft Matter Systems. *Comput. Phys. Commun.* 174:704–727.

5. Grest, G. S., and K. Kremer, 1986. Molecular-Dynamics Simulation for Polymers in the Presence of a Heat Bath. *Phys. Rev. A* 33:3628–3631.

6. Harmandaris, V. A., and M. Deserno, 2006. A novel method for measuring the bending rigidity of model lipid membranes by simulating tethers. *J. Chem. Phys.* 125:204905.

7. Theodorou, N., Doros, and U. W. Suter, 1985. Shape of unperturbed linear polymers: polypropylene. *Macromol.* 18:1206–1214.

8. van Kampen, N. G., 2007. Stochastic Processes in Physics and Chemistry. Elsevier, Amsterdam, 3 edition.

9. Press, W. H., S. A. Teukolsky, W. T. Vetterling, and B. P. Flannery, 2007. Numerical Recipes. Cambridge University Press, New York, 3 edition.

10. Cuvelier, D., I. Derényi, P. Bassereau, and P. Nassoy, 2005. Coalescence of membrane tethers: experiments, theory, and applications. *Biophys. J.* 88:2714–2726.

11. Rowlinson, J. S., and B. Widom, 2002. Molecular Theory of Capillarity. Dover, New York, 1 edition.

12. Helfrich, W., 1981. Physics of Defects. North Holland, Amsterdam.

13. Helfrich, W., 1994. Lyotropic Lamellar Phases. *J. Phys. Condens. Matt.* 6:A79–A92.

14. Szleifer, I., D. Kramer, A. Ben-Shaul, W. M. Gelbart, and S. A. Safran, 1990. Molecular theory of curvature elasticity in surfactant films. *J. Chem. Phys.* 92:6800–6817.

15. Irving, J. H., and J. G. Kirkwood, 1950. The statistical mechanical theory of transport processes. 4. The equations of hydrodynamics. *J. Cchem. Phys.* 18:817–829.

16. Schofield, P., and J. R. Henderson, 1982. Statistical Mechanics of Inhomogeneous Fluids. *Proc. R. Soc. Lond. A* 379:231–246.

17. Wajnryb, E., A. R. Altenberger, and J. S. Dahler, 1995. Uniqueness of the microscopic stress tensor. *J. Cchem. Phys.* 103:9782–9787.